

Fulde-Ferrell state induced purely by the orbital effect in a superconducting nanowire

Paweł Wójcik,^{1,*} Michał Zegrodnik,^{2,†} and Józef Spałek^{3,2,‡}

¹*AGH University of Science and Technology, Faculty of Physics and Applied Computer Science,
30-059 Krakow, Poland* Al. Mickiewicza 30, 30-059 Krakow, Poland

²*Academic Centre for Materials and Nanotechnology,*

AGH University of Science and Technology, Al. Mickiewicza 30, 30-059 Krakow, Poland

³*Marian Smoluchowski Institute of Physics, Jagiellonian University, ul. Łojasiewicza 11, 30-348 Kraków, Poland*

(Dated: 10.05.2015)

We show that the Fulde-Ferrell (FF) phase may appear as a sole result of the orbital effect in a cylindrical metallic nanowire. Namely, in the external magnetic field the two-fold degeneracy with respect to the orbital magnetic quantum number m is lifted, what leads to a Fermi wave vector mismatch between the subbands with opposite orbital momenta in the paired state. This mismatch can be compensated by the nonzero total momentum of the Cooper pairs created by electrons from the split subbands what results in the formation of the FF phase. In this manner, a transformation of the orbital motion into a linear supercurrent parallel to the applied field is taking place. With the increasing magnetic field a series of FF stability regions appear, in between which the standard BCS superconducting phase is stable. For the sake of completeness, we show, that the inclusion of the Zeeman term in the model does not change the picture qualitatively, particularly if larger m states contribute essentially to the Fermi-surface splitting. A brief but important note concerning the possibility of steering the supercurrent by an applied magnetic field parallel to it, is also provided.

PACS numbers: 74.78.Na, 84.71.Mn

I. INTRODUCTION

According to the original concept by Fulde and Ferrell¹ (FF), as well as by Larkin and Ovchinnikov² (LO), a superconducting phase with nonzero center-of-mass momentum of the Cooper pairs can be induced by the Zeeman spin splitting of the Fermi surface which appears in the external magnetic field. The Fermi wave vector mismatch, caused by this Fermi surface splitting, is detrimental to the pairing, but can be compensated by the emerging nonzero total-momentum of the Cooper pairs. This allows for the superconducting phase to persist in magnetic fields substantially higher than the second critical field H_{c2} . In order to make it possible for the resultant non-zero momentum Cooper pairing to appear, several requirements are to be met. First of all, the Maki parameter³ should be large meaning that the Pauli paramagnetic effect has to be strong relative to the orbital pair-breaking mechanism.⁴ Moreover, the system has to be very clean as the FFLO phase is easily destroyed by the presence of impurities.⁵ Because of those rather stringent conditions there are not many examples for such nonzero-momentum pairing to occur. Until now, the experimental signs of the FFLO state have been suggested for the organic superconductors^{6–9} and the heavy fermion compound CeCoIn_5 .^{10–12} The quasi-two-dimensional structure of those systems leads to a strong reduction of the orbital pair breaking in the applied in-plane magnetic field, as well as to nesting properties of the quasi-2D Fermi surface. Both of these features are expected to stabilize the FFLO phase.

An indirect experimental evidence of nonzero-momentum pairing has been recently reported for a system consisting of ultracold ^6Li atoms trapped in

an array of one dimensional tubes.^{13–15} One should also note the ongoing theoretical investigations regarding the appearance of the FFLO state in other systems such as heavy fermion superconductors with spin-dependent masses,^{16,17} iron pnictides,^{18,19} ultracold fermionic atoms,^{20–22} as well as layered^{23–25} and quasi-one dimensional²⁶ superconductors.

We consider here the case of a metallic cylindrical nanowire and demonstrate that the orbital effect, which so far has been regarded as detrimental to the FFLO phase formation, can in fact induce the nonzero-momentum paired state. This situation is facilitated in a unique manner by the transfer of kinetic energy from the rotational to the translational degrees of freedom. Namely, the rotational degrees of freedom lead to the Fermi surface splitting since in the applied field the states with the magnetic quantum numbers m and $-m$ have opposite magnetic moments what in turn results in opposite energy contributions. The Fermi wave-vector mismatch created by the splitting is transferred into the nonzero total momentum of the Cooper pairs along the nanowire inducing the FF phase formation. We also provide an argument for a feasibility of such state observability.

The structure of the paper is as follows. In the next Section we determine the quasiparticle states in the wire with nontrivial azimuthal states (i.e., in the direction perpendicular to its length) within a modified Bardeen-Cooper-Schrieffer (BCS) approach, in which the superconducting gap acquires an explicit angular momentum dependence. We also specify explicitly how the Fermi wave vector mismatch arises solely from the angular-momentum induced Fermi surface splitting. The self-consistent equation for the gap, together with that determining the chemical potential for the fixed carrier con-

centration, are also specified. In Section III we discuss our results, as well as predict concrete experimentally verifiable effects of sandwiching the FF states in the sequence of the BCS-type states with the increasing applied magnetic field. Finally, Sec. IV is devoted to a brief summary and a general discussion to what extent the proposed effect can be useful in creating/modifying the supercurrent in quantum-electronics devices. Additionally, some details concerning the derivation of the self-consistent equations for the superconducting gap and the chemical potential are deferred to the Appendix A, whereas the elementary determination of the superconducting parameters is provided in Appendix B, together with a direct interpretation of our results.

II. MODEL

We start with introducing the cylindrical coordinates (r, φ, z) and choosing the gauge for the vector potential as $\mathbf{A} = (0, eH_{||}r/2, 0)$, where the magnetic field $H_{||}$ is parallel to the nanowire axis. Then the single-electron Hamiltonian in the cylindrical nanowire then has the following form

$$\hat{H}_0 = \frac{\hbar^2}{2m_e} \left[-\frac{1}{r} \frac{\partial}{\partial r} r \frac{\partial}{\partial r} + \left(-\frac{i}{r} \frac{\partial}{\partial \varphi} + \frac{eH_{||}r}{2\hbar} \right)^2 - \frac{\partial^2}{\partial z^2} \right], \quad (1)$$

where m_e is the electron mass and e is the electron charge. To underline the role of orbital degrees of freedom we have neglected the Zeeman term which complicates unnecessarily the analysis (the argument remains of the same type). For the sake of completeness, at the end of Sec. III we show, that the inclusion of the Zeeman term does not change the results qualitatively. Hamiltonian (1) is simplified further due to the negligible role of the diamagnetic term $\sim \mathbf{A}^2$ which for nanowires is one order of magnitude lower than that of the order parameter. In the nanowire geometry the quantization of the single-electron energy into a series of subbands appears. These subbands are indexed by the orbital magnetic m and radial j quantum numbers, what leads to the dispersion relations

$$\xi_{k,m,j} = \frac{\hbar^2 \gamma_{m,j}^2}{2m_e R^2} + \frac{\hbar^2 k^2}{2m_e} + m\mu_B H_{||} - \mu, \quad (2)$$

where k is the particle momentum along the nanowire (z axis), $\gamma_{m,j}$ is the j -th zero of the m -th order Bessel function, R is the nanowire radius, and μ is the chemical potential. The corresponding single electron wave functions have the form

$$\phi_{kmj}(r, \varphi, z) = \frac{1}{2\pi} \tilde{J}_{mj}(r) e^{im\varphi} e^{ikz}, \quad (3)$$

where $\tilde{J}_{mj}(r)$ is defined as

$$\tilde{J}_{mj}(r) = \frac{\sqrt{2}}{RJ_{m+1}(\gamma_{m,j})} J_m\left(\frac{\gamma_{m,j}}{R} r\right), \quad (4)$$

with $J_m(r)$ being the m -th order Bessel function. One should note that $\xi_{k,m,j} = \xi_{k,-m,j}$ for $H_{||} = 0$.

Next, we include the effective electron-electron attraction term in the model and perform the BCS approximation with the possibility of non-zero momentum pairing (with the momentum q along the z -axis). The BCS Hamiltonian is then of the form

$$\hat{H} = \sum_{kmj} \xi_{k,m,j} \hat{n}_{k,m,j} + \sum'_{mj} \frac{|\Delta_{mj}|^2}{V} + \sum'_{kmjq} (\Delta_{mj} \hat{c}_{k,m,j\uparrow}^\dagger \hat{c}_{-k+q,-m,j\downarrow}^\dagger + H.C.), \quad (5)$$

where V is the coupling constant and Δ_{mj} is the superconducting (SC) gap defined by

$$\Delta_{mj} = \frac{V}{4\pi^2} \sum'_{km'j'} C_{mj m'j'} \langle \hat{c}_{-k+q,-m',j\downarrow} \hat{c}_{k,m',j\uparrow} \rangle, \quad (6)$$

with the gap modulation

$$C_{mj m'j'} = \int_0^R dr \, r \tilde{J}_{mj}^2(r) \tilde{J}_{m'j'}^2(r). \quad (7)$$

The primed summation means that m runs over the nonnegative values only. Additionally, for the summation over k , the pairing appears only in the range $[\mu - \hbar\omega_D, \mu + \hbar\omega_D]$, where ω_D is the Debye frequency. From Eq. (5) one can see that for $q = 0$ the pairing appears within each subband labelled with the radial quantum number j between particles with opposite spins, momenta, and orbital momenta: $(k, m, j \uparrow; -k, -m, j \downarrow)$. So the pairing contains both the translational and the rotational degrees of freedom. In the applied field the degeneracy with respect to m is removed resulting in a shift between the subbands corresponding to m and $-m$ [cf. Eq. (2)]. In such situation, a Fermi-wave-vector mismatch appears. However, this mismatch can be transferred into the nonzero center-of-mass momentum of the Cooper pairs ($q \neq 0$) giving rise to the FF phase induced purely by the orbital effect. This process is represented in Fig. 1. For simplicity, we limit to the situation in which all the Cooper pairs have a single momentum q constituting the Fulde-Ferrell phase.

Diagonalization of (5) leads to the quasiparticle energies

$$E_{kmjq}^\pm = \pm \frac{1}{2} (\xi_{k,m,j} - \xi_{-k+q,-m,j}) + \sqrt{\frac{1}{4} (\xi_{k,m,j} + \xi_{-k+q,-m,j})^2 + \Delta_{mj}^2}. \quad (8)$$

The set of self-consistent equations for the SC gap parameter and the chemical potential have the corresponding form

$$\Delta_{mj} = \frac{V}{4\pi^2} \int dk \sum'_{mj} C_{mj m'j'} \times \frac{\Delta_{mj} [1 - f(E_{kmjq}^+) - f(E_{kmjq}^-)]}{\sqrt{(\xi_{m,j,k} + \xi_{-k+q,-m,j})^2 + 4\Delta_{mj}^2}}, \quad (9)$$

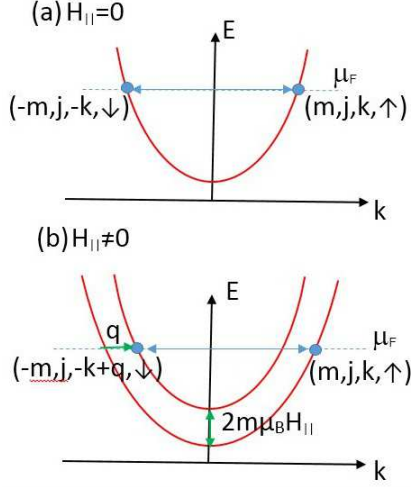


FIG. 1. Schematic representation of Cooper paired states in the nanowire. (a) BCS case, (b) FF pairing. The horizontal arrow connects the pair partners, for which the sets of quantum numbers are specified in the brackets.

$$n_e = \frac{1}{\pi^2 R^2} \int dk \sum'_{mj} \int_0^R dr r \{ |u_{kmjq}(r)|^2 f(E_{kmjq}^+) + |v_{kmjq}(r)|^2 [1 - f(E_{kmjq}^-)] \}, \quad (10)$$

where n_e is the electron concentration and $f(E)$ is the Fermi-Dirac distribution. One should note that Eqs. (6) and (9) correspond to the SC gap in reciprocal space. Also, in the standard BCS theory the chemical potential is regarded as the same in the normal and superconducting phases. Here, as the confinement can significantly affect the chemical potential, we prefer to adjust it in each of the phases (normal and superconducting) separately, as it should be in principle. Details concerning the derivation of the self-consistent equations are contained in the Appendix at the end of the paper.

The confinement in the radial directions of the nanowire leads to the r dependence of the SC gap which is determined by

$$\Delta_q(r) = \frac{V}{4\pi^2} \int dk \sum'_{mj} v_{kmjq}^*(r) u_{kmjq}(r) \times [1 - f(E_{kmjq}^+) - f(E_{kmjq}^-)], \quad (11)$$

where $u_{kmjq}(r) = U_{kmjq} \tilde{J}_{mj}(r)$ and $v_{kmjq}(r) = V_{kmjq} \tilde{J}_{mj}(r)$, with U_{kmjq} , V_{kmjq} being the Bogoliubov coherence factors, which in turn are elements of the diagonalization matrix of (5).

The SC gaps Δ_{mj} and the chemical potential are obtained by solving Eqs. (9) and (10) numerically, whereas the wave-vector q is determined by minimizing the free energy of the system.²⁷ Additionally, by using Eq. (11) the spatial dependence of the gap can be determined explicitly.

III. RESULTS

Calculations have been carried out for the following values of the parameters: $\hbar\omega_D = 32.31$ meV, $gN(0)=0.18$, where $N(0) = \frac{mk_F}{2\pi^2\hbar^2}$ is the bulk density of states at the Fermi level, $\Delta_{bulk} = 0.25$ meV and $\mu_{bulk} = 0.9$ eV which corresponds to the electron density $n_e = 3.88 \times 10^{18} \text{ cm}^{-3}$. The selected parameter values correspond to Al superconductor.²⁸ To determine

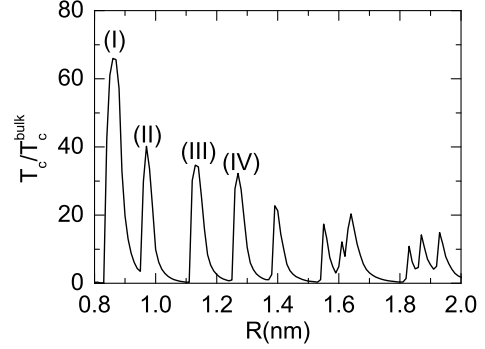


FIG. 2. Superconducting critical temperature T_c/T_c^{bulk} as a function of nanowire radius R . The analysis of the unconventional paired phase proposed in this work is carried out for R corresponding to the maxima labeled by I, II, III, and IV. Note that the same results have been obtained in Ref. 28 (cf. Fig. 1).

the values of R which are appropriate for the analysis of the proposed unconventional paired phase, we have calculated the nanowire radius dependence of the critical temperature in zero magnetic field. The T_c oscillations seen in Fig. 2 have identical form as those presented in Ref. 28 and result from the electrons energy quantization due to the confinement effect. Maximum of the T_c appears each time an electron subband passes through the energy window $[\mu_F - \hbar\omega_D, \mu_F + \hbar\omega_D]$. In what follows, the possibility of non-zero momentum pairing due to the orbital effect is analyzed for the values of the nanowire radius which correspond to the maxima (shape resonances) labeled by I-IV in Fig. 2.

In Fig. 3 we show the magnetic field dependence of the averaged superconducting gap

$$\bar{\Delta} = \frac{1}{R} \int_0^R \Delta(r) dr, \quad (12)$$

for the value of R corresponding to T_c maximum labeled by II. As one can see from Eq. (2), the orbital pair breaking mechanism caused by the Fermi surface splitting has different magnitude for bands corresponding to different values of $|m|$. As a result, the zero temperature superconducting-to-normal metal transition driven by the magnetic field occurs as a cascade of jumps in the order parameter as displayed in Fig. 3(a). It has been reported in Ref. 29 that each jump corresponds to Cooper

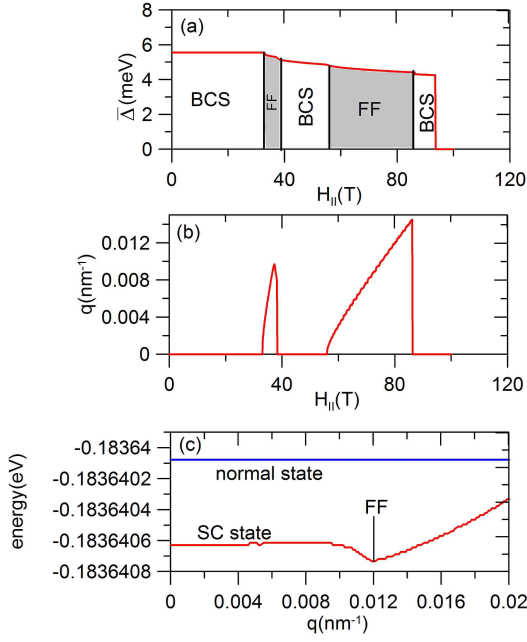


FIG. 3. (a) Magnetic field dependence of the averaged superconducting gap; (b) total Cooper pair momentum which minimizes the energy vs. $H_{||}$; (c) Cooper pair momentum dependence of the energy in the paired and normal states for selected value of the field. The energy minimum visible in (c) corresponds to the stability of FF phase. Results for $R = 0.97$ nm labeled by II in Fig. 2.

pair breaking in a subsequent subband. Here, we show that the Fermi wave vector mismatch, which appears in individual bands due to the orbital effect, can be compensated by nonzero center-of-mass momentum of the Cooper pairs leading to the FF phase appearance. It is shown in Fig. 3(a) that the stability of the FF phase appears for certain ranges of $H_{||}$ in between which the BCS phase is stable. In Fig. 3(c) we show the minimum in the q -dependence of the system energy for the selected value of external magnetic field which corresponds to the stability of the FF state.

The structure of the FF and BCS stability ranges (cf. Fig. 3) is caused by the multiband nature of the system. It should be noted that the contributions to the paired phase coming from different subbands, which is defined as (cf. Eq. (11))

$$P_{m,j}(r) = \frac{V}{4\pi\Delta_q(r)} \int dk v_{kmjq}^*(r) u_{kmjq}(r) \times \left[1 - f(E_{kmjq}^+) - f(E_{kmjq}^-) \right],$$

may vary significantly. In Fig. 4(a-c) we present the quasiparticle branches for subbands (m,j) participating in the SC state, as well as the r -dependence of the SC gap for the selected radius R in zero field. By analyzing $\Delta(r)$ [Fig. 4(b)] and $P_{m,j}(r)$ [Fig. 4(c)] one can conclude that for the selected resonant radius, there is a

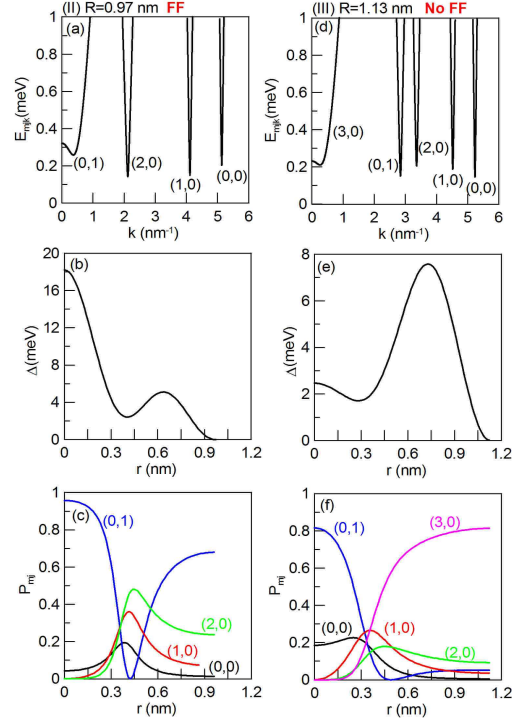


FIG. 4. (a,d) Quasi-particle subbands labeled by (m,j) participating in SC state; (b,e) r -dependence of the SC gap $\Delta(r)$; (c,e) contributions to the paired phase coming from different subbands. Results are for $R = 0.97$ nm (II - left panels) and $R = 1.13$ nm (III - right panels), both for $H_{II} = 0$.

leading quasiparticle branch e.g. $(0,1)$ for $R = 0.97$ nm (corresponding to the energy gap $\Delta_{0,1}$) that controls the superconducting gap enhancement. The dominant contribution to the SC state, which comes solely from single branch is a characteristic feature of each resonant radius.²⁸ The critical field, $H_{||c}$, at which the transition SC-normal metal appears, is mainly determined by such dominant energy gap. The remaining quasiparticle branches are responsible for the appearance of the FF-state stability ranges seen in Fig. 3(a). Their influence on the formation of the FF phase can be explained as follows. As already mentioned, the impact of the applied magnetic field on different subbands is dependent on the orbital quantum number $|m| \neq 0$. The larger $|m|$, the faster the Fermi wave vector mismatch rises with increasing $H_{||}$ (cf. Eq. 2). In effect, the depairing in the subbands with different $|m|$ takes place for different $H_{||}^m$. Close to $H_{||}^m$ the Fermi wave vector mismatch between the paired electrons $|(k, m, j, \uparrow), (-k, -m, j, \downarrow)\rangle$ is compensated by the non-zero total momentum of the Cooper pairs leading to the stable FF phase. However, upon further increase of the field it is not possible to adjust the vector q so as to sustain the pairing in such subband and the Cooper pairs in this subband break up leading to a decrease of the energy gap and standard BCS pairing reentrance. This allows to formulate the

conditions for the appearance of the FF stability regimes induced by the orbital effect in nanowires. Namely, the FF phase appears only if the dominant quasi-particle branch has the orbital quantum number lower than the other superconducting branches excluding those with $m = 0$. The number of FF stability regions is equal to the number of the subbands which fulfill this criterion. From Fig. 4 one can see that for $R = 0.97$ nm there are two subbands (1,0) and (2,0) (subbands with $m = 0$ are excluded) with a larger quantum number than the dominant subband (0,1). This results in two FF stability regions shown in Fig. 3(a) with different slopes of $q(H_{II})$, (Fig. 3(b)) depending on the orbital quantum number $|m|$ corresponding to branches responsible for the $q \neq 0$ paired phase. As one can see in Fig. 5, the FF

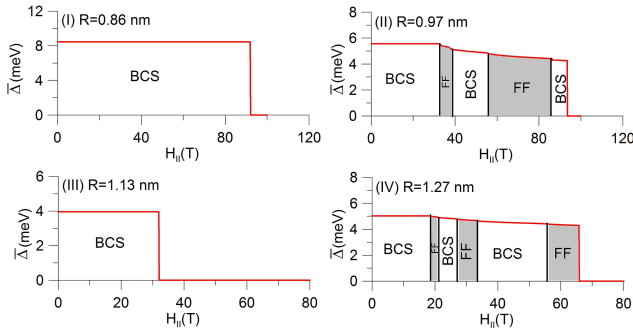


FIG. 5. Magnetic field dependences of the averaged SC gap for four nanowire radii corresponding to resonances I-IV, respectively.

stability does not always appear with increasing field. Such situation takes place when the dominant band corresponds to large value of $|m|$ and the depairing in this band appears before it does in other quasiparticle branches. The quasiparticle dispersion relations in such case ($R = 1.13$ nm, (III)) are shown in Fig. 4 together with the corresponding r dependence of the averaged gap parameter and the contributions to the pairing coming from particular subbands. As one can see, for $R = 1.13$ nm the largest contribution to the pairing originates from the subband with $m = 3$ and $j = 0$. Due to relatively large value of m , the corresponding quasiparticle branch reaches zero energy before any other and as a result, the FF state induced by the less important branches does not appear.

Zeeman effect. To underline the role of the orbital effect in the creation of the FF state in nanowires, the results presented so far did not include the influence of the spin Zeeman term. However, it should be noted that the Pauli paramagnetism is the second factor being able to create the FF phase in nanowires. The extension of our theoretical model for the case with the spin Zeeman effect included, leads in a straightforward manner to the spin-dependent dispersion relations in the form analogous

to Eq. (2), namely

$$\xi_{k,m,j,\sigma} = \frac{\hbar^2 \gamma_{m,j}^2}{2m_e R^2} + \frac{\hbar^2 k^2}{2m_e} + m\mu_B H_{||} + \sigma\mu_B H_{||} - \mu, \quad (13)$$

where $\sigma = \pm 1$ for spin-up and down electrons, respectively. Diagonalization of (5) with the dispersion relations (13) leads to the quasiparticle energies in the form

$$E_{kmj}^{\pm} = \pm \frac{1}{2}(\xi_{k,m,j,\uparrow} - \xi_{-k+q,-m,j,\downarrow}) + \sqrt{\frac{1}{4}(\xi_{k,m,j,\uparrow} + \xi_{-k+q,-m,j,\downarrow})^2 + \Delta_{mj}^2} \quad (14)$$

In Fig. 6 we present the stability diagrams calculated for the four nanowire radii I-IV, with the inclusion of the spin Zeeman effect. As can be seen the obtained results

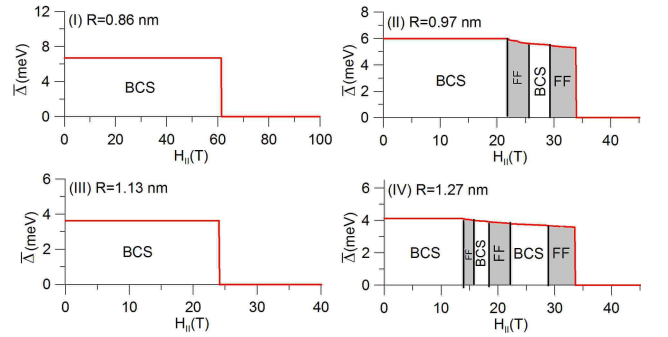


FIG. 6. Magnetic field dependences of the averaged SC gap for four nanowire radii (I)-(IV) calculated with the inclusion of the spin Zeeman effect.

do not differ qualitatively from the corresponding ones presented in Fig. 5. The FF stability regions induced by the orbital effect are still clearly visible. Nevertheless, as one can expect, the Zeeman effect reduces the value of the critical magnetic field (cf. Figs. 5 and 6). Its impact is crucial especially for resonances governed by the low orbital quantum numbers $m = 0, 1$; e.g. for $m = 0$ the orbital effect is not operative and only the Pauli paramagnetism determines the value of the corresponding critical magnetic field. By comparing Figs. 5 and 6 one can see that the largest reduction of the critical field is obtained for $R = 0.97$ nm which corresponds to the resonance governed by the state with $m = 0$ (cf. Fig. 4). It should be noted that the inclusion of the spin Zeeman effect does not alter the conclusion that for the states with higher orbital quantum number, which participate in the formation of the superconducting phase (cf. Fig. 4), the depairing takes place for the lower values of the magnetic field giving raise to the stable FF phase. For the resonances governed by the higher orbital quantum number m the spin Zeeman effect does not play the crucial role and to the first approximation it is negligible. For example, the reduction of the critical field for $R = 1.13$ nm, governed by $m = 3$, is much less pronounced.

IV. SUMMARY AND OUTLOOK

The orbital effect (i.e. the Fermi-surface dependence on the orbital magnetic quantum number, m) in cylindrical superconducting nanowires results in the Fermi wave-vector mismatch which can be transferred to the nonzero linear momentum of the Cooper pairs. By solving the system of Bogoliubov-de Gennes equations numerically, we have shown that this effect leads to stability of the FF phase in certain ranges of the applied magnetic field oriented parallel to the nanowire. The nonzero total momentum of the Cooper pairs is induced to sustain the pairing in the corresponding subbands what in turn leads to structure of alternating FF and BCS stability ranges as shown in Figs. 3 and 4. To expose the role of the orbital effect in the formation of the FF phase, we have first neglected the usual spin-Zeeman term in our approach. However, for the sake of completeness, calculations with the inclusion of the Pauli paramagnetism have also been carried out subsequently and show no significant qualitative differences with respect to the case without the spin Zeeman term included (cf. Figs. 5 and 6).

The proposed mechanism of the FF phase formation induced by the orbital effect appears only if few states with different quantum numbers participate in the superconducting phase. At the same time, the thicker the nanowire is, the more states take part in the pairing. As a consequence, our analysis is restricted to relatively thin nanowires. Nevertheless, by lowering the electron concentration we also decrease the number of states taking part in the pairing. As shown in one of our previous papers,³⁰ this fact leads to the increase of T_c oscillations as a function of sample size for nanofilms (the same holds true for nanowires). This fact allows us to suggest that for a superconductor with low concentration of carriers, e.g., for SrTiO₃³¹, the presented effect may be observed also for much thicker nanowires.

By carrying out the specific heat measurements one could detect if the phase transitions between the FF and BCS phases, shown in Figs. 5 and 6, appear with the increasing magnetic field. Moreover, one should note, that in the FF phase the Cooper pairs have nonzero total momentum which in our case leads to a supercurrent flow along the nanowire induced by a parallel to it magnetic field. This fact can also be used as a signal in the experimental detection of the proposed effect, as well as can have practical consequences in quantum-electronic devices, in the sense that the current can be created and stimulated by magnetic field applied parallel to its direction.

For simplicity, we have analyzed nanowires with a uniform cross section. One should note that the effect of sample nonuniform cross section can make the experimental observation of the FF state obscured, since the energy gain coming from the nonzero momentum pairing is rather small [cf. Fig. 3(c)]. On the other hand, a strong enhancement of the T_c value with respect to that for a bulk sample should make the effect observable for

uniform wires in the clean limit.

Finally, a methodological remark is in place here. The quantum wires considered in this paper have a non-trivial dynamics in the dimensions perpendicular to its length. Therefore, such systems cannot be regarded as strictly one-dimensional. This is the reason why we do not consider them from the electronic point of view as Tomanaga-Luttinger liquids. The question whether superconducting 1D liquids can produce the proposed effect, is still open.

V. ACKNOWLEDGEMENT

This work was financed from the budget for Polish Science in the years 2013-2015, project number: IP2012 048572. M. Z. and J. S. acknowledge the financial support from the Foundation for Polish Science (FNP) within the project TEAM. J. S. acknowledges also the Grant MAESTRO from the National Science Center (NCN), No. DEC-2012/04/A/ST3/00342.

APPENDIX A: EFFECTIVE BCS HAMILTONIAN FOR THE NANOWIRE

In this Appendix we present some details of the effective BCS Hamiltonian derivation for the superconducting nanowire in an external magnetic field. Moreover, we also show how to obtain the self-consistent equations for the gap parameter and the chemical potential.

We start from the general form of the BCS Hamiltonian

$$\begin{aligned} \hat{\mathcal{H}} = & \sum_{\sigma} \int d^3r \hat{\Psi}^{\dagger}(\mathbf{r}, \sigma) \hat{H}_0 \hat{\Psi}(\mathbf{r}, \sigma) \\ & + \int d^3r \left[\Delta(\mathbf{r}) \hat{\Psi}^{\dagger}(\mathbf{r}, \uparrow) \hat{\Psi}^{\dagger}(\mathbf{r}, \downarrow) + H.C. \right] \\ & + \int d^3r \frac{|\Delta(\mathbf{r})|^2}{V}, \end{aligned} \quad (15)$$

where \hat{H}_0 is the single-electron Hamiltonian, in our case defined by (1), and the gap parameter in real space is given by

$$\Delta(\mathbf{r}) = -V \left\langle \hat{\Psi}(\mathbf{r}, \downarrow) \hat{\Psi}(\mathbf{r}, \uparrow) \right\rangle. \quad (16)$$

For the case of cylindrical nanowire we chose the field operators in the form

$$\begin{aligned} \hat{\Psi}(\mathbf{r}, \sigma) &= \sum_{kmj} \phi_{kmj}(\mathbf{r}) \hat{c}_{kmj\sigma}, \\ \hat{\Psi}^{\dagger}(\mathbf{r}, \sigma) &= \sum_{kmj} \phi_{kmj}^*(\mathbf{r}) \hat{c}_{kmj\sigma}^{\dagger}, \end{aligned} \quad (17)$$

where $\phi_{kmj}(\mathbf{r})$ are the eigenfunctions of \hat{H}_0 and are given by Eq. (3). For the case of superconducting nanowire

the Cooper pairs are created by electrons with opposite spins and angular momenta. Additionally, we assume that the pairs can have nonzero total momentum, q , along the nanowire. In such situation, by substituting Eqs. (16) and (17) into Eq. (15), one obtains the effective Hamiltonian in the form defined by Eq. (5). Next, by introducing the composite vector operators $\hat{\mathbf{f}}_{kmjq}^\dagger = (\hat{c}_{k,m,j\uparrow}^\dagger, \hat{c}_{-k+q,-m,j\downarrow}^\dagger)$ and assuming that all the Cooper pairs have a single momentum q (the Fulde-Ferrell phase), we arrive at the following form of the effective Hamiltonian

$$\hat{H} = \sum'_{kmj} \hat{\mathbf{f}}_{kmjq}^\dagger \mathbf{H}_{kmjq} \hat{\mathbf{f}}_{kmjq} + \sum'_{kmj} \xi_{-k+q,-m,j} + \sum'_{mj} \frac{|\Delta_{mj}|^2}{V}, \quad (18)$$

where

$$\mathbf{H}_{kmjq} = \begin{pmatrix} \xi_{k,m,j} & \Delta_{mj} \\ \Delta_{mj}^* & -\xi_{-k+q,-m,j} \end{pmatrix}, \quad (19)$$

and Δ_{mj} is defined via Eq. (9). Hamiltonian (18) can be diagonalized by the use of the Bogoliubov transformation to new quasiparticle operators $\hat{\alpha}_{k,m,j,q}$ and $\hat{\beta}_{k,m,j,q}$, which has the following form

$$\begin{pmatrix} \hat{c}_{k,m,j\uparrow}^\dagger \\ \hat{c}_{-k+q,-m,j\downarrow}^\dagger \end{pmatrix} = \begin{pmatrix} U_{kmjq} & V_{kmjq} \\ -V_{kmjq}^* & U_{kmjq} \end{pmatrix} \begin{pmatrix} \hat{\alpha}_{k,m,j,q} \\ \hat{\beta}_{k,m,j,q}^\dagger \end{pmatrix}, \quad (20)$$

where

$$U_{kmjq} = \frac{1}{2} \left(1 + \frac{\xi_{k,m,j} + \xi_{-k+q,-m,j}}{\sqrt{(\xi_{k,m,j} - \xi_{-k+q,-m,j})^2 + 4\Delta_{mj}^2}} \right),$$

$$V_{kmjq} = \frac{1}{2} \left(1 - \frac{\xi_{k,m,j} + \xi_{-k+q,-m,j}}{\sqrt{(\xi_{k,m,j} - \xi_{-k+q,-m,j})^2 + 4\Delta_{mj}^2}} \right), \quad (21)$$

are the Bogoliubov coherence factors. The columns of the unitary transformation matrix from Eq. (20) are the eigenvectors of the matrix form of our Hamiltonian (19). After the diagonalization transformation, the Hamiltonian has the following form

$$\hat{H} = \sum'_{kmj} (E_{kmjq}^+ \hat{\alpha}_{k,m,j,q}^\dagger \hat{\alpha}_{k,m,j,q} + E_{kmjq}^- \hat{\beta}_{k,m,j,q}^\dagger \hat{\beta}_{k,m,j,q}) + \sum'_{kmj} (\xi_{-k+q,-m,j} - E_{kmjq}^-) + \sum'_{mj} \frac{|\Delta_{mj}|^2}{V}, \quad (22)$$

where E_{kmjq}^\pm are given by Eq. (8)

The self-consistent equation for the superconducting gap (9) can be derived by substituting for $\hat{c}_{-k+q,-m,j\downarrow}$ and $\hat{c}_{k,m,j\uparrow}$ from Eq. (20) into Eq. (6). Similarly, the equation for the chemical potential (10) is obtained by

inserting the creation and annihilation operators from (20) into the equation for the electron concentration

$$n_e = \frac{2}{\Omega} \int dk \sum_{mj} \langle \hat{n}_{k,m,j} \rangle, \quad (23)$$

where Ω is the system volume. It should be noted that with the use of the self-consistent equation (6) one obtains the superconducting gap in reciprocal space. After solving the self-consistent equations, the position dependence of the gap can be calculated in a straightforward manner by inserting the field operators (17) into Eq. (16) and then using the Bogoliubov transformation (20).

APPENDIX B: ELEMENTARY ESTIMATE OF THE SUPERCONDUCTING NANOWIRE PARAMETERS AND ADDITIONAL PHYSICAL COMMENTS

A brief note concerning the experimental situation is in place here. The experimental evidence for superconductivity appearance in the thinnest nanowires of radius $R \sim 1$ nm in not clearly established³² even though for thicker nanowires the T_C value grows with the decreasing diameter. In particular, the role of the order-parameter quantum fluctuations has been discussed as a detrimental factor³³ in the case of zero field. Here we have considered relatively thin wires and have shown that a stable BCS or FF states can appear even for $R \sim 1$ nm and in strong fields. Such state of affairs can be understood within the following semi-macroscopic picture emerging from the Ginzburg-London type of approach³⁴ in which we treat the nanowire as a 3-dimensional cylinder filled with electron gas and do not include the quantum size effect explicitly. The London penetration depth $\lambda_L = (m_0 c^2 / e^2 n_c)^{1/2}$ is for the low carrier concentration $n_c \sim 4 \cdot 10^{18} \text{ cm}^{-3}$ of the order of 10^3 nm, i.e., much larger than the wire diameter. On the other hand, the coherence length $\xi = \hbar^2 k_F / (m^* \Delta)$, where k_F is the Fermi wave vector, is much smaller than λ_L and is of the order of R . Hence, we have the superconductor of extreme type II. Note that bulk Al is the superconductor of type I. The difference appears because for the wire the carrier concentration is about 4 orders of magnitude smaller and in this situation, the values of the $\lambda_L \sim 1/n_c$ and $\xi \sim \hbar k_F \sim n_c^{1/3}$ will be vastly different. It should also be noted that in nanostructures the coherence length can be suppressed even more due to the quantum size effect³⁵. Under the circumstance that the field penetrates the whole sample, we can estimate the second critical field, which is $H_{c2} = \Phi_0 / 2\pi \xi^2$, where Φ_0 is the flux quantum. Explicitly, $H_{c2} \sim 10^2$ T, whereas the first critical field $H_{c1} \equiv \Phi_0 / (4\pi \lambda_L^2) \ln(\xi / \lambda_L) \sim 10^{-3}$ T. Note that the fields, at which the FF state appears (cf. Figs 3(a), 5, and 6) are in the similar interval, explicitly $10 - 100$ T. Therefore, one may ask whether the flux lines do not form along the wire direction instead of the FF state.

This seems not feasible because the wire is long and too thin as we have assumed at the start. Explicitly, the size of the London orbit is $l_0 = (\Phi_0/2\pi H_a)^{1/2}$ and equals to $l_0 = 3\text{nm}$ and 2nm for $H_a = 50\text{T}$ and 100T , respectively. In such case the FF state is formed, with the supercurrent density $j_s = |e|n_c(\hbar q/m^*)$ and stabilizes the superconducting state, as the Cooper pair total momentum compensates the Fermi wave vector mismatch. Taking $q \sim 0.01\text{nm}^{-1}$ (cf. Fig. 3c) we obtain the supercurrent $I = j_s \pi R^2$, which for $R = 1\text{nm}$ amounts to the value $\sim 1\mu\text{A}$. The pair velocity in FF state is $\hbar q/m^* \sim 10^3\text{m/s}$, whereas the Fermi velocity is about $7 \cdot 10^5\text{m/s}$, so the velocity of a steady Cooper-pair flow is much smaller than the Fermi velocity. One should note that such current in turn produces the magnetic field at the wire surface of the magnitude $B = \mu_0 I/(2\pi R) \sim 10^{-4}\text{T}$, i.e., far below the order of magnitude of the applied field. As a result, the magnetic field induced by the supercurrent in the FF state does not compensate the applied field

which causes the Fermi wave vector mismatch. Obviously, this is a mean-field (BCS-like) picture which should most probably be amended by the discussion of the order-parameter fluctuation effects, since the coherence length is rather small. Nonetheless, the present discussion provides a coherent overall picture, as well as justifies our assumption that the field is uniform within the sample volume. Obviously, we assume that the wire cross section is uniform, presumably monocrystalline, and in the clean limit. Perhaps, the ring configuration would be the best for experiments, since in such geometry the Fulde-Ferrell phase is more appropriate than a formation of the Larkin-Ovchinnikov supercurrent standing-wave state.

Parenthetically, the physical situation is reminiscent of what takes place in the case of high-temperature superconductors. It is thus tempting to suggest an experiment on wires (or rather, thin stripes) composed of a high-temperature superconductor.

-
- * pawel.wojcik@agh.edu.pl
† michal.zegrodnik@agh.edu.pl
‡ ufspalek@if.uj.edu.pl
- ¹ P. Fulde and A. Ferrell, Phys. Rev. **135**, A550 (1964).
 - ² A. I. Larkin and Y. N. Ovchinnikov, Zh. Eksp. Teor. Fiz. **47**, 1136 (1964).
 - ³ D. Saint-James, G. Sarma, and E. J. Thomas, *Type II Superconductivity* (Pergamon, New York, 1969).
 - ⁴ L. W. Gruenberg and L. Gunther, Phys. Rev. Lett. **16**, 996 (1966).
 - ⁵ S. Takada, Prog. Theor. Phys. **43**, 27 (1970).
 - ⁶ J. Singleton, J. A. Symington, M. S. Nam, A. Ardavan, M. Kurmoo, and P. Day, J. Phys. Condens. Matter **12**, L641 (2000).
 - ⁷ M. A. Tanatar, T. Ishiguro, H. Tanaka, and H. Kobayashi, Phys. Rev. B **66**, 134503 (2002).
 - ⁸ S. Uji, T. Terashima, M. Nishimura, Y. Takahide, T. Konoike, K. Enomoto, H. Cui, H. Kobayashi, H. Kobayashi, A. nad Tanaka, M. Takumoto, E. S. Choi, T. Tokumoto, D. Graf, and J. S. Brooks, Phys. Rev. Lett. **97**, 157001 (2006).
 - ⁹ J. Shinagawa, Y. Kurosaki, F. Zhang, C. Parker, S. E. Brown, D. Jerome, J. B. Christensen, and K. Bechgaard, Phys. Rev. Lett. **98**, 147002 (2002).
 - ¹⁰ A. Blanchi, R. Movshovich, C. Capan, P. G. Pagluso, and J. L. Sarrao, Phys. Rev. Lett. **91**, 187004 (2003).
 - ¹¹ K. Kumagai, M. Saitoh, T. Oyaizu, Y. Furukawa, S. Takashima, M. Nohara, H. Takagi, and Y. Matsuda, Phys. Rev. Lett. **97**, 227002 (2006).
 - ¹² V. F. Correa, T. P. Murphy, C. Martin, K. M. Purcell, E. C. Palm, G. M. Schmiedenshoff, J. C. Cooley, and W. Tozer, Phys. Rev. Lett. **98**, 087001 (2007).
 - ¹³ Y. Liao, A. S. C. Rittner, T. Paprotta, W. Li, G. B. Partridge, R. G. Hulet, S. K. Baur, and E. J. Mueller, Nature **467**, 567 (2010).
 - ¹⁴ K. Sun and C. J. Bolech, Phys. Rev. A **85**, 051607(R) (2012).
 - ¹⁵ K. Sun and C. J. Bolech, Phys. Rev. A **87**, 053622 (2013).
 - ¹⁶ J. Kaczmarczyk and J. Spalek, J. Phys. Condens. Matter **22**, 355702 (2010).
 - ¹⁷ M. M. Maška, M. Mierzejewski, J. Kaczmarczyk, and J. Spalek, Phys. Rev. B **82**, 054509 (2010).
 - ¹⁸ A. Ptok and D. Crivelli, J. Low Temp. Phys. **172**, 226 (2013).
 - ¹⁹ A. Ptok, Eur. Phys. J. B **87**, 2 (2014).
 - ²⁰ F. Wu, G. C. Guo, W. Zhang, and W. Yi, Phys. Rev. Lett. **110**, 110401 (2013).
 - ²¹ X. J. Liu and H. Hu, Phys. Rev. B **87**, 051608(R) (2013).
 - ²² L. Dong, L. Jiang, and H. Pu, New J. Phys. **15**, 075014 (2013).
 - ²³ M. D. Croitoru, M. Houzet, and A. I. Buzdin, Phys. Rev. Lett. **108**, 207005 (2012).
 - ²⁴ M. D. Croitoru and A. I. Buzdin, Phys. Rev. B **86**, 064507 (2012).
 - ²⁵ M. D. Croitoru and A. I. Buzdin, J. Phys. Condens. Matter **25**, 125702 (2013).
 - ²⁶ M. D. Croitoru and A. I. Buzdin, Phys. Rev. B **89**, 224506 (2014).
 - ²⁷ I. Kosztin, S. Kos, M. Stone, and A. J. Legget, Phys. Rev. B **58**, 9365 (1998).
 - ²⁸ A. A. Shanenko and M. D. Croitoru, Phys. Rev. B **73**, 012510 (2010).
 - ²⁹ A. A. Shanenko, M. D. Croitoru, and F. M. Peeters, Phys. Rev. B **78**, 024505 (2008).
 - ³⁰ P. Wójcik and M. Zegrodnik, phys. stat. sol. (b) **251**, 1069 (2014).
 - ³¹ J. F. Schooley, W. R. Hosler, and M. L. Cohen, Phys. Rev. Lett. **12**, 474 (1964).
 - ³² M. Zgirski, K.-P. Riikonen, V. Touboltsev, and K. Arutyunov, Nano Lett. **5**, 1029 (2005).
 - ³³ M. Zgirski, K.-P. Riikonen, V. Touboltsev, and K.-Y. Arutyunov, Phys. Rev. B **77**, 054508 (2008).
 - ³⁴ M. Cyrot and D. Pavuna, *Introduction To Superconductivity And High-Tc Materials* (World Scientific Publishing Co. Pte. Ltd., Singapore, 1992).
 - ³⁵ A. A. Shanenko, M. D. Croitoru, A. Vagov, and F. M. Peeters, Phys. Rev. B **82**, 104524 (2010).